Int. J. Nanosci. Nanotechnol., Vol. 17, No. 4, Dec. 2021, pp. 239-248

Rational Design of Phosphorus Abundant Co_2P Nanoparticles Encapsulated by Nitrogen-doped Carbon Nanotubes for Superior Lithium Ion Capacitors with 4.5 Voltage

Juan Xu* and Haibin Guo

North China University of Water Resources and Electric Power, Zhengzhou 450000, PR China

(*) Corresponding author: xujuan@ncwu.edu.cn
(Received: 11 June 2021 and Accepted: 15 November 2021)

Abstract

The sluggish reaction kinetics and aggregation of volume during lithiation/delithiation process are the main obstacles of anode for li-ion capacitors (LICs). Here, we use the "three bird one stone" strategy to design the anode of phosphorus abundant Co_2P nanoparticles encapsulated by N-doped CNTs rationally. The Co_2P nanoparticles contribute to shorten the Li^+ diffusion length, while abundant phosphorus guaranteeing the high electrical conductivity and N-CNTs providing stable structure protecting layers. Hence, Co_2P/N-CNTs electrode reveals a large specific capacity of 807 mAh g^{-1} at 0.1 A g^{-1} over 200 cycles and excellent rate performance of 395 mAh g^{-1} at 3.2 A g^{-1}. Extraordinary, the capacitive contribution of Co_2P/N-CNTs electrode at 1 mV s^{-1} is 80.73%, contributing to the enhanced reaction kinetics and rate capacity. The LICs comprising of Co_2P/N-CNTs anode and activated carbon (AC) cathode demonstrate an outstanding energy density of 130 Wh kg^{-1} at 625 W kg^{-1} along with 90.24% capacity retention over 10000 cycles at 5 A g^{-1} within 4.5 V. The proposed strategy can be applied to develop promising electrode materials for promising energy storage systems.

Keywords: *Co_2P/N-CNTs, Anode, three bird one stone, High rate capacity, High ratio of capacitive contribution capacity.*

1. INTRODUCTION

Since the 21C, researchers around the world in the field of energy storage systems have paid great attention to li-ion batteries (LIBs) owing to the increasing demand of high energy density and long cycling life [1-3]. Generally, LIBs exhibit high specific capacity but suffer from sluggish charging/discharging rate capacity comparing with the power-type energy storage device of supercapacitors (SCs). However, SCs store energy by the electric double-layer or pseudocapacitance mechanisms in electrodes, which can't fulfill the requirements of devices with high energy density [4-8]. Therefore, focused studies are recently on the li-ion capacitors (LICs) integrating high energy density obtained by the faradaic process on anode and large power density achieved via the electric double layer effect on cathode. In addition, organic electrolyte containing Li^+ providing wide working voltage window was recognized as an appropriate choice for LICs due to its low cost and similar performance compared with the Li counterpart [10-13]. Recently, metal phosphorous (eg : FeP [14], NiP_3 [15], SnP_3 [16], CuP_2 [17], and CoP_x [18]) have been chosen as ones of the most promising anode of LICs, in view of their high specific capacity and low discharge voltage plateau.

Among various types of CoP_x, the orthorhombic Co_2P demonstrates better structure stability and higher electrical conductivity owing to the more Co element and metallic character, which is the promising anode candidate of LICs. However, the development of Co_2P-based

electrodes in LICs still restricted by the large volumetric expansion, severe particle aggregation and poor electrical conductivity during the lithiation/delithiation process [19-24].

To tackle these problems, one promising strategy is to integrate Co_2P with conductive carbon materials [27-30]. The hybrid structure can not only prevent the agglomeration of active materials and enhance the electric conductivity, but also alleviate the large volume expansion, thereby improving the overall electro-chemical performances of electrode. Although some advances have been made in recent years, the li-ion storage performance of these hybrids is still unsatisfied, mainly due to the poor interfacial contact between the transition-metal phosphides and carbon materials. Therefore, designing innovative architect-ure able to provide more intimate interfacial contact between transition-metal phosphides and conductive carbon and simultaneously to prevent the aggregation of nanoparticles remains the great challenge.

In this paper, the novel structure of Co_2P nanoparticles encapsulated by porous carbon polyhedral composed of N-doped carbon nanotubes (Co_2P/N-CNTs) was achieved via facile solvent-thermal method with subsequent phosphorization treatment. Distinctly, the Li^+ diffusion coefficient and capacitive-controlled energy storage ratio at high sweep rates are significantly rein-forced by strong synergistically coupling of Co_2P nanoparticle units and the surrounding N-doped CNTs network. In addition, Co_2P nanoparticles offer numerous active sites and large specific surface areas, which effectively reduce the Li^+ diffusion length and increase the availability of electrolyte ions. Also the N-doped CNTs network acts as the fast outer electrons transport layer and protective layers of the stable structure during lithiation/delithiation process. Therefore, Co_2P/N-CNTs electrode exhibit a large discharging capacity of 807 mAh g^{-1} at 0.1 A g^{-1} over 200 cycles along with high Coulombic efficiency nearly 100% at each cycle, excellent rate performance of 395 mAh g^{-1} at 3.2 A g^{-1} , which is evaluated to be the promising anode of high performance LICs. Based on the perfect match of Co_2P/N-CNTs anode and AC cathode, high performance LICs are constructed, which demonstrated an outstanding energy density of 130 Wh kg^{-1} at 625 W kg^{-1} along with a reasonable stable cycling of 90.24% capacity retention over 10000 cycles at 5 A g^{-1} within the voltage of 4.5 V.

2. EXPERIMENT

2.1. Material Preparation

Co_2P/N-CNTs composites were achieved by a facile solvent-thermal treatment followed by phosphorization in Ar. The precursor of ZIF-67 was synthesized in the previous report [31]. Then the resulting precipitates of ZIF-67 were annealed at 900 °C for 4 h with the heating rate of 5 °C min^{-1} under N_2, which were named as Co-MOF/N-CNTs. After carbonization, the obtained products of Co-MOF/N-CNTs and NaH_2PO_2 with the ratio from 1:5 to 1:20 were put into two different boats and heated at 350 °C for 2 h with the heating rate of 2 °C min^{-1} in Ar flow. Finally, the products were washed with deionized water and ethanol for several times until the solution being transparent and dried at 60 °C in oven overnight.

2.2. Material Characterization

The morphology of products was charactered by field-emission scanning electron microscopy (FE-SEM, FEI Nova NanoSEM 450) and high resolution transmission electron microscopy (HR-TEM, FEI Tecnai G20). The crystal structure was performed by Powder X-ray diffraction (XRD) (PANanalytical B.V., Netherlands) with Cu Kα radiation (λ = 1.5418 Å). X-ray photoelectron spectroscopy (XPS, Kratos AXIS Ultra DLD-600 W) and Raman scattering (InVo-RENISHAW) were further analysed to achieve the chemical bonds and structural

composition of the materials. The specific surface area was evaluated by N_2 adsorption-desorption isotherms (Micromeritics ASAP 2020 analyzer). Thermal analysis (STA449) was conducted to analyse the carbon content in Co_2P/N-CNTs. All the electrochemical tests were carried out by electrochemical workstations (CHI760E, Shanghai, China) and battery test system (Xinwei, Shenzhen, China).

2.3. Electrochemical Measurements

Fabrication of Li-ion half cells: The working electrodes were prepared as follows: 75% active material, 10% binder (Polyvinylidene Fluoride) (PVDF) and 15% conductive additive (super P) were mixed in N-methyl-2-pyrrolidone (NMP) solution uniformly with stirring overnight to form the slurry. The slurry was coated on a copper foil/aluminum foil serving as the current collector followed by vacuum drying at 80 °C overnight. Li-ion half cells were prepared in an argon-filled glove box with Li foil serving as the counter electrode, using 1.0 M $LiPF_6$ in a 1:1 vol/vol mixture of ethylene carbonate (EC) and diethyl carbonate (DEC) with 5% Fluoroethylenecarbonate (FEC) as the electrolyte, and glass fiber membrane (GF/D, Whatman) as the separator.

Fabrication of LICs: Prior to construct the LICs, the Co_2P/N-CNTs electrode was preactivated for three cycles at 0.1 A g^{-1} with lithium foil as the counter electrode. Afterwards, the prelithiated Co_2P/N-CNTs anode and activated carbon (AC) cathode were assembled into the LICs using the same separator and electrolyte in li-ion half cells.

Electrochemical Measurement: The specific capacitance (C, F g^{-1}) of half-cells and LICs were calculated by Equation (1)

$$C = I\,\Delta t/(m\,\Delta V) \quad (1)$$

where I is constant current (A), Δt represents the discharging time (s), m is the mass of the active materials based on anode and cathode (g) and ΔV represents the working voltage window (V), respectively. In addition, the energy density (E, Wh kg^{-1}) of a LIC is achieved by Equation (2)

$$E = 1/2\,CV^2 \quad (2)$$

where C is the specific capacitance based on Equation (1) and V is the working voltage window. The power density (P, W kg^{-1}) of the LIC is determined by the energy density (E) and discharging time (t) according to Equation (3).

$$P = E/t \quad (3)$$

3. RESULTS AND DISCUSSION

The Co_2P/N-CNTs composites can be achieved by the facile solvent-thermal process and following phosphorization treatment, which is displayed in Scheme 1. Firstly, ZIF-67 was synthesized by the self-assembly of Co^{2+} ions and 2-methylimidazole in methanol at room temperature as the precursor. Secondly, the precursor was annealed in N_2 to enhance the structure stability and conductivity, which named as Co-MOF/N-CNTs. Finally, the Co_2P/N-CNTs hybrid was achieved by phosphidation of the as-prepared Co-MOF/N-CNTs with NaH_2PO_2 under Ar atmosphere with the optimum mass ratio of 1: 15.

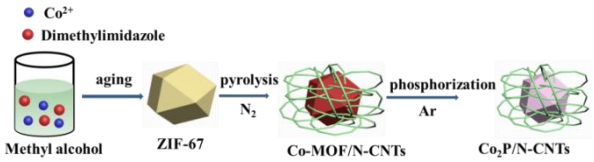

Scheme 1 *Material synthesis process of Co_2P/N-CNTs employed for the anode of li ion capacitors (LICs).*

Figure 2 presents the morphology of Co_2P/N-CNTs composites. Excellent structure of porous carbon polyhedron composed of N-doped CNTs wrapped Co_2P nanoparticles is clearly observed in Figure 2a-2c. Co_2P/N-CNTs composites possess uniform rhombic dodecahedral-like morphology with average size of 300 nm; the Co_2P nanoparticle unit with a diameter of approximately 80 nm and surrounded by a large number of intertwined CNTs. The microstructure of Co_2P/N-CNTs is further

investigated by transmission electron microscopy (TEM) measurement. Figure 2d reveals that the

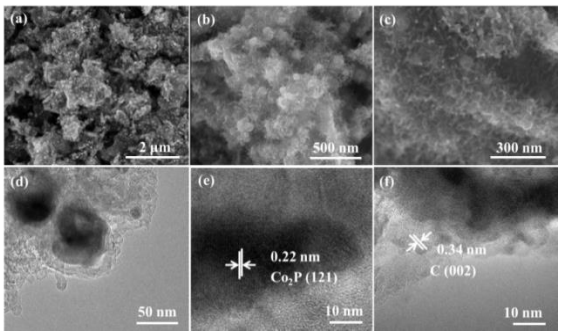

Figure 2. *(a,b,c) SEM images of Co_2P/N-CNTs; (d) TEM micrograph of Co_2P/N-CNTs highlighting the morphology of the Co_2P nanoparticles and surrounding N-CNTs network; (e,f) HRTEM images of Co_2P/N-CNTs emphasis on inter-spacing of Co_2P and N-CNTs, respectively.*

CNTs with the length of a few hundred nanometers and diameters of 30 nm homogeneously surround the Co_2P nanoparticles. The lattice fringe of 0.22 nm can be assigned to the (121) plane of Co_2P and the lattice fringe of 0.34 nm can be indexed to the (002) plane of graphic carbon (Figure 2e-2f), respectively. Also, there exists amorphous carbon of CNTs.

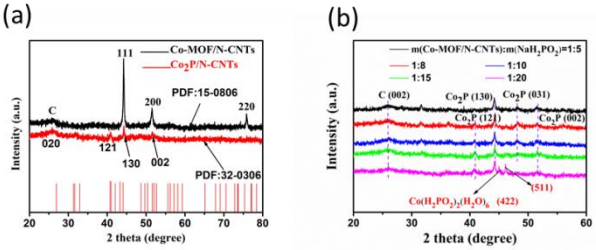

Figure 3. *(a) X-ray diffraction (XRD) of Co_2P/N-CNTs and Co-MOF/N-CNTs; (b) XRD patterns of the products with the source quality ratio of Co-MOF/N-CNTs to NaH_2PO_2 from 1:5 to 1:20.*

The crystal structure of Co_2P/N-CNTs was achieved by X-ray diffraction (XRD) shown in Figure 3a. Specifically, the strong peaks located at 40.8°, 44.3° and 51.6° can be indexed to the (121), (130) and (002) planes of orthorhombic Co_2P/N-CNTs (JCPDS card No. 32-0306). Additionly, the peak located at 25.8° is the (020) plane of carbon, which is consistent with the TEM in Figure 2f. Also, the peaks at 44.2°, 51.6° and 75.9° corresponds to the (111), (200) and (220) planes of Co-MOF/N-CNTs (JCPDS card No. 15-0806). Apparently, these peaks are belong to metallic Co. We further study the effects of quality ratio of sources on products in Figure 3b. When the quality ratio of Co-MOF/N-CNTs to NaH_2PO_2 been 1/5, 1/8, 1/10, the Co-MOF/N-CNTs can't be phosphated completely, because of the peak at 44.2° belonging to metallic Co still remained. However, new peaks appears at 44.1°, 46.2° when the ratio is 1/20, which belongs to the (422) and (511) plane of cubic $Co_2(H_2PO_2)_2(H_2O)_6$ (JCPDS card No. 01-075-0031), respectively. Therefore, 1/15 was selected as the optimal phosphation quality ratio of Co-MOF/N-CNTs to Co_2P/N-CNTs.

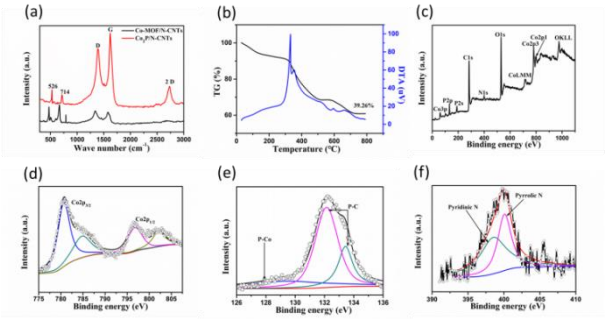

Figure 4. *(a) Raman patterns of Co_2P/N-CNTs and Co-MOF/N-CNTs; (b) TG curves of Co_2P/N-CNTs from 0 to 800℃ ; (c) X-ray photoelectron (XPS) spectra obtained from Co_2P/N-CNTs of the (d) Co 2p, (e) P 2p, (f) N 1s.*

Figure 4a performs the typical Raman spectra of Co_2P/N-CNTs, while the peaks centered at 526 and 714 cm^{-1} can be indexed as the typical Raman active 2LA (M) and A1g vibrational modes of Co_2P, respectively [32]. In addition, the peaks at 1388 and 1620 cm^{-1} are ascribed to the D and G band of N-CNTs, with the I_D/I_G value obtained at about 0.88, indicating that there are abundant defects and graphitic carbon in

the Co_2P/N-CNTs, which contributes to the high conductivity and mass active sites [10]. The nitrogen adsorption-desorption isotherms showed the mesoporous characteristics of Co_2P/N-CNTs (Figure S1). The BET specific surface area is 190 m^2 g^{-1} and pore volume is 0.36 cm^3 g^{-1}. Figure S2 shows the mesopores size distribution centered at around 18.5 nm. It is believed that the high specific surface area and large porous volume provide plenty of interfaces and mass transport pathways to enhance the fast diffusion of Li^+ during the charging/discharging cycles. Figure 4b showed the thermogravimetric (TGA) results in the 0-800℃ temperature range, the Co_2P/N-CNTs is decomposed to yield Co_3O_4 in the air in the end. According to the calculation, the mass ratio of Co_2P is 56.48% in the Co_2P/N-CNTs. The surface chemistry of Co_2P/N-CNTs was investigated by X-ray photoelectron spectroscopy (XPS) (Figure 4c), which including Co, P, N, C and O species. As shown in Figure 4d, Co 2p core-level XPS spectrum of Co_2P/N-CNTs can be deconvoluted into two peaks centered at 780.5 and 797.6 eV, which belong to the typical Co $2p_{3/2}$ and Co $2p_{1/2}$, respectively. It is consistent with the state of Co 2p in Co_2P. In addition, the high-resolution P 2p spectrum of Co_2P/N-CNTs in Figure 4e reveals the presence of P-Co bonding and P-C bonding, which stated at 128 eV and 132 eV, 133.4 eV, respectively [20-23]. The deconvoluted high-resolution N 1s spectra of Co_2P/N-CNTs are centered at 398.2 eV, 399.6 eV, in association with pyridinic N, pyrrolic N in the Co_2P/N-CNTs (Figure 4f) [33]. Additionly, the C 1s and O 1s spectra showed in Figure S3 and S4, which confirmed the existence of C and O in Co_2P/N-CNTs.

The electrochemical performance of Co_2P/N-CNTs electrode was evaluated to judge its potential as a promising anode of LICs. Figure 5a depicts the cyclic voltammetry (CV) measurements of the initial five cycles of Co_2P/N-CNTs electrode at the scan rate of 0.1 mV s^{-1}. In the first cathodic scan process, a broad reduction peak can be observed at about 1.02 V, which can be assigned to irreversible reaction related to the formation of solid electrolyte interface (SEI).

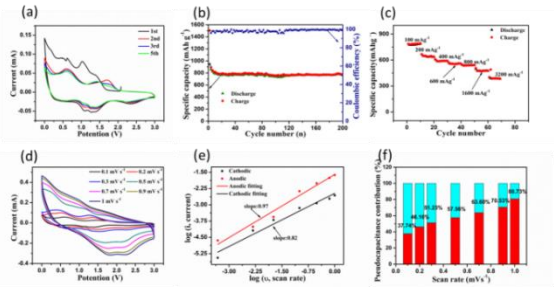

Figure 5. *The electrochemical performance of Co_2P/N-CNTs electrode: (a) Cycling performance at the current density of 0.1 A g^{-1} for the 1st, 2nd, 3rd, 5th cycle; (b) The specific capacity at 0.1 A g^{-1} over 200 cycles. (c) Rate properties; (d) CV curves at 0.1, 0.2, 0.3, 0.5, 0.7, 0.9, 1 mV s^{-1}; (e) Specific peak current at a series scan rates from 0.1 to 1 mV s^{-1}; (f) CV curves with separation between total current (blue area) and capacitive current (red area) at 1 mV s^{-1}.*

In addition, there are two distinct major peaks at 1.26 V and 0.52 V, which should attributed to the conversion reaction of Co_2P with Li^+ ions into Co metallic nanoparticles embedded into Li_3P matrix as illustrated in Equation (1) [16-20].

$$3Li^+ + 3e^- + Co_2P \leftrightarrow 2\,Co + Li_3P \qquad (1)$$

In the first anodic scan, two main broad oxidation peaks located at 1.26 V and 2.24 V should be ascribed to the decomposition of Li_3P. Interestingly, the almost overlapping CV curves of Co_2P/N-CNTs electrode from the 2nd to 5th sweeps show higher reversible conversion and enhanced stability of electronic transport upon the lithiation/delithiation process. Figure S5 shows the galvanostatic charge-discharge (GCD) curves of Co_2P/N-CNTs electrode at 0.1 A g^{-1} with unobvious voltage plateau, demonstrating dominating capacitive-controlled energy storage. Figure 5b

displays the charging/discharging cycling performance of Co_2P/N-CNTs electrode at 0.1 A g^{-1}. The charge and discharge capacities of Co_2P/N-CNTs electrode in the 1st cycle are 896 and 1480 mAh g^{-1}, respectively, corresponding to an initial Coulombic Efficiency (CE) of about 60.5%. The irreversible capacity loss during the first discharge-charge process is mainly due to the formation of SEI on the surface of the electrode [10]. However, the CE of the electrode increases rapidly, and the following discharge/charge curves are almost exactly overlapped with each other, demonstrating high reversibility. Surprisingly, Co_2P/N-CNTs electrode exhibits about 807 mAh g^{-1} at 0.1 A g^{-1} over 200 cycles, displaying high specific capacity and excellent cycling stability. Besides, Co_2P/N-CNTs electrode also show enhanced rate capability. As demonstrated in Figure 5c, the electrode was examined at the current density from 0.1 to 3.2 A g^{-1}. Surprisingly, Co_2P/N-CNTs electrode can still retain 406 mAh g^{-1} at the ultrahigh current density of 3.2 A g^{-1}, which is superior to previous reports of Co_2P as the anode for Li-ion half-cells. Additionally, Co_2P/N-CNTs electrode remained nearly 400 mAh g^{-1} at the high current density of 3.2 A g^{-1} over 1000 cycles in Figure S6, demonstrating high rate capacity. So, it was the promising anode of LIC. From the electrochemical impedance spectroscopy (EIS) data expressed in Figure S7, it is clearly seen that the Co_2P/N-CNTs electrode has the small charger transfer resistance over 10000 charging/discharging cycles. Improved Li^+ diffusion coefficient and electrons transport rate could be ascribed to the unique electrons transfer network constructed by Co_2P nanoparticle units and high conductive N-CNTs network. To further explore the kinetics process of Co_2P/N-CNTs electrode, a series of CV curves at the sweep rates from 0.1 to 1 mV s^{-1} are performed in Figure 5d. It clearly displays that the obvious positive shift in anodic peaks and negative shift in cathodic peaks with the increasing of scan rates, demonstrating significant polarization during lithiation/delithiation process. The Li^+ transport kinetics of Co_2P/N-CNTs electrode can be analysed by Equation (2) to achieve the dominant effect of diffusion-controlled redox reaction or surface capacitive process.

$$i=av^b \quad (2)$$

where a and b are variable constant, v is the scan rate. The b equals to 1 indicating a capacitive process, while b of 0.5 shows a semi-infinite diffusion process dominated by Li^+ insertion [28]. As illustrated in Figure 5e, b is 0.82 and 0.97 for cathodic and anodic peaks of Co_2P/N-CNTs electrode at the scan rates less than 1 mV s^{-1}, respectively, which shows a dominant surface capacitive process. It clearly revealed that the effect of diffusion process is more and more prominent with the increasing of scan rates. We can calculate the relative contribution of the capacitive process by comparing the shaded area with the entire stored charges by the Equation (3).

$$i=k_1\upsilon+k_2\upsilon^{1/2} \quad (3)$$

where k_1 and k_2 are constant, υ is the scan rate, $k_1\upsilon$ is the surface capacitive-controlled process and $k_2\upsilon^{1/2}$ is the diffusion-controlled process [34]. As a result, Figure 5f exhibits 80.73% of the total capacity at 1 mV s^{-1} (red region) achieved by the surface capacitive process, demonstrating dominant capacitive contribution in Co_2P/N-CNTs electrode during lithiation/delithiation process. In detail, Figure 5f shows the relative ratio of capacitive contribution at the scan rates from 0.1 to 1.0 mV s^{-1}. With the increasing of scan rates, the ratio of capacitive contribution enlarges from 37.74% to 80.73%, which may attributed to the enhanced reaction kinetics and more pseudocapacitive reactive sites at the surface and near-surface region of the optimized Co_2P/N-CNTs electrode.

We constructed the LICs using prelithiated Co_2P/N-CNTs anode and AC

cathode to power the laptop and electric bus and the proposed charge-storage mechanism is shown in Figure 6a.

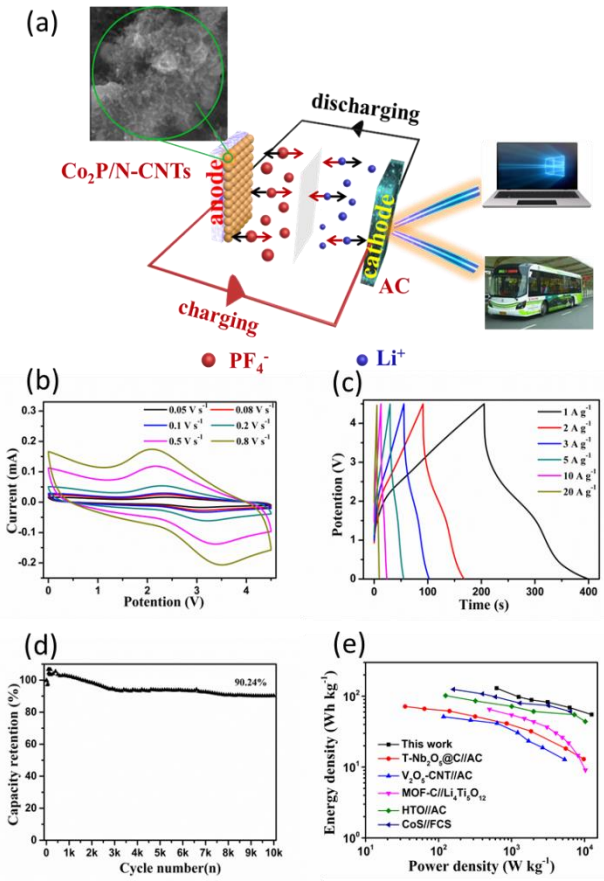

Figure 6. *(a) Schematic illustration of the assembled LICs; (b) CV curves of the LICs at various scan rates; (c) GCD curves of the LICs at various current densities; (d) Cycling performance at 5 A g^{-1} for 10000 cycles; (e) Ragone plots of the Co_2P/N-CNTs//AC LICs comparing with other LIC systems.*

During the charging process, PF_4^- ions are adsorbed on the surface and defect sites of AC cathode, while Li^+ ions insert into the Co_2P/N-CNTs anode [10]. Additionally, the discharging process is in contrary of the charging process. Prior to assemble the LICs, the Co_2P/N-CNTs anode was preactivated with proceeding 2 cycles at 0.1 A g^{-1} then discharging to 0.2 V to achieve a wide working voltage window and eliminate the initial irreversible reaction. Being benefited from the safe electrolyte working potential and the voltage profiles of Co_2P/N-CNTs and AC electrodes, the maximum voltage window of the LIC is likely to be 4.5 V. With the increasing of the voltage window to 4.5 V, the specific capacity of LIC increased. Considering that the amplitude of the capacity in Co_2P/N-CNTs anode and AC cathode will not change in line with the increase of current density, the mass ratio of active materials in anode and cathode should be optimized. Combining the Equation (4) with the CV curves and GCD curves, we can conclude that 1:3.5 is the optimal mass ratio of anode and cathode [10].

$$Q^+ = C^+ \times m^+ = Q^- = C^- \times m^- \quad (4)$$

Figure 6b shows the CV curves of Co_2P/N-CNTs//AC LIC at the scan rates from 50 to 800 mV s^{-1} in the working voltage of 0.0-4.5 V with the mass ratio of anode and cathode being 1:3.5. The CV curves exhibit similar rectangular shape, perfectly coupling with the Capacitor-type and Faradaic-type energy storage process at the cathode and anode, respectively. With the increasing of scan rates, the rectangular shape of CV curves is still maintained without severe deformation, demonstrating high cycling reversibility and good rate capability. The GCD curves of Co_2P/N-CNTs//AC LIC at the current densities from 1 to 20 A g^{-1} show linear slope with the Coulombic Efficiency nearly 100% (Figure 6c). According to the calculation, the corresponding specific capacity (based on the total active mass of anode and cathode) are 44.4, 35.6, 33.3, 32.4, 30.8 and 29.8 F g^{-1} at the high current densities of 1, 2, 3, 5, 10, 20 A g^{-1}, respectively. Furthermore, the Co_2P/N-CNTs//AC LIC achieves an outstanding cycling stability with 90.24% capacity retention over 10000 charging/discharging cycles at the current density of 5 A g^{-1} along with the Coulombic Efficiency nearly 100% (Figure 6d). Importantly, the Co_2P/N-CNTs//AC LIC obtains the maximum energy density of 130 Wh kg^{-1} at the power density of 625 W kg^{-1}. Even at the high-power output of 12500

W kg^{-1}, the LICs still maintain an extraordinary energy density of 55 Wh kg^{-1}. The higher energy density and power density of the Co_2P/N-CNTs//AC LIC surpass several previously reported LICs, such as T-Nb_2O_5@C//AC [35], V_2O_5-CNT//AC [36], MOF-C//$Li_4Ti_5O_{12}$ [37], HTO//AC [38], CoS//FCS [39]. With this superior electrochemical performance, the Co_2P/N-CNTs//AC LICs are regarded as the promising candidate to power hybrid electric vehicles easily.

4. CONCLUSIONS

In summary, the hierarchical porous Co_2P/N-CNTs were developed by a facile approach, which can be realized with the aid of solvent-thermal process and phosphorization in Ar. As-prepared Co_2P/N-CNTs show the integrated advantages of hierarchical porous structure as well as high electrical conductivity and stable structure protecting layer of N-doped CNTs network. According to the calculations, Co_2P/N-CNTs electrode exhibits capacitance-controlled charge storage process especially at the higher scan rates. As a consequence, Co_2P/N-CNTs electrode displays outstanding rate capability and ultra-long cycling stability over 200 cycles, regarding as the promising anode of high performance LICs. On this basic, high performance LICs using Co_2P/N-CNTs anode and AC cathode is assembled, which delivers high energy density at large power density and extraordinary cycling stability within the wide voltage window of 4.5 V. Our synthetic strategy integrates the advantages of metal phosphide and CNTs and can used to prepare other electrode materials. Also, the high performance Co_2P/N-CNTs anode and AC cathode may provide a convenient way to obtain advanced LICs.

CONFLICT OF INTEREST

The authors declare that they have no known competing financial interests or personal relationships that could have appeared to influence the work reported in this paper.

ACKNOWLEDGEMENT

This research was supported by the Doctoral Research Grant funded by the North China University of Water Resources and Electric Power.

REFERENCES

1. Hosseini, S. A., Saghfi, M., Abiri, H., "Comparision of binary and ternary compositions of Ni-Co-Cu oxides/VACNTs electrodes for energy storage devices with excellent capacitive behavior", *J. Nanosci. Nanotechnol.*, 16 (2020) 91-102.
2. Tabassum, H., Zou, R. Q., Mahmood, A., Liang, Z. B., Wang, Q. F., Zhang, H., Gao, S., Qu, C., Guo, W. H., GuO, S. J., "A universal strategy for hollow metal oxide nanoparticles encapsulated into B/N co-doped graphitic nanotubes as high-performance lithium-ion battery anodes", *Adv. Mater.*, (2018) 1705441.
3. Shang, T. T., Wen, Y. R., Xiao, D. D., Gu, L., Hu, Y. S., Li, H., "Atomic-scale monitoring of electrode materials in lithium-ion batteries using in situ transmission electron microscopy", *Adv. Energy Mater.*, (2017) 1700709.
4. Xu, J., Li, C. Y., Chen, L. L., Li, Z. Y., Bing, P. B., "Anchoring carbon layers and oxygen vacancies endow WO_{3-x}/C electrode with high specific capacity and rate performance for supercapacitors", *RSC Adv.*, 9 (2019) 28793.
5. Xu, J., Ding, T. T., Wang, J., Zhang, J., Wang, S., Chen, C. C., Fang, Y. Y., Wu, Z. H., Huo, K. F., Dai, J. N., "Tungsten oxide nanofibers self-assembled mesoscopic microspheres as high-performance electrodes for supercapacitor", *Electrochim. Acta.*, 174 (2015) 728-734.
6. Zheng, S. S., Xue, H. G., Pang, H., "Supercapacitors based on metal coordination materials", *Coordination Chemistry Reviews*, 373 (2018) 2-21.
7. Li, Q., Xu, Y. X., Zheng, S. S., Guo, X. T., Xue, H. G., Pang, H., "Recent progress in some amorphous materials for Supercapacitors", *Small*, 14 (2018) 1800426.
8. Wang, K. B., Xun, Q., Zhang, Q. C., "Recent progress in metal-organic frameworks as active materials for supercapacitors", *Energychem*, 2 (2020) 100025.
9. Xu, J., Li, Y. Y., Wang, L., Cai, Q. F., Li, Q. W., Gao, B., Zhang, X. M., Huo, K. F., Chu, P. K., "High-energy lithium-ion hybrid supercapacitors composed of hierarchical urchin-like WO_3/C anodes and MOF-derived polyhedral hollow carbon cathodes", *Nanoscale*, 8 (2016) 16761.
10. Xu, J., Liao, Z. H., Zhang, J. B., Gao, B., Chu, P. K., Huo, K. F., "Heterogeneous phosphorus-doped WO_{3-x}/nitrogen-doped carbon nanowires with high rate and long life for advanced lithium-ion capacitors", *J. Mater. Chem. A*, 6 (2018) 6916-6921.

11. Xu, J., Gao, B., Huo, K. F., Chu, P. K., "Recent progress in electrode materials for nonaqueous lithium-ion capacitors", *J. Nanosci. Nanotechnol.*, 20 (2020) 2652-2667.
12. Yan, W., Su, J., Yang, Z. M., Lv, S., Jin, Z., Zuo, J. L., "High-performance lithium-ion capacitors based on porosity-regulated zirconium metal-organic frameworks", *Small*, 17 (2020) 2005209.
13. Zuo, W. H., Li, R. Z., Zhou, C., Li, Y. Y., Xia, J. L., Liu, J. P., "Battery-supercapacitor hybrid devices: recent progressand future prospects", *Adv. Sci.*, (2017) 1600539.
14. Yang, Y., Fu, W., Lee, D. C., Bell, C., Drexler, M., Ma, Z. F., Magasinski, A., Yushin, G., Alamgir, F. M., "Porous FeP/C composite nanofibers as high-performance anodes for Li-ion/Na-ion batteries", *Materials Today Energy*, 16 (2020) 100410.
15. Fullenwarth, J., Darwiche, A., Soares, A., Donnadieu, B., Monconduit, L., "NiP_3: a promising negative electrode for Li- and Na-ion batteries", *J. Mater. Chem. A*, 2 (2014) 2050-2059.
16. Park, J. W., Park, C. M., "Electrochemical li topotactic reaction in layered SnP_3 for superior li-ion batteries", *Scientific Reports*, 6 (2016) 35980.
17. Kim, S. O., Manthiram, A., "Phosphorus-rich CuP_2 embedded in carbon matrix as a high performance anode for lithium-ion batteries", *ACS Appl. Mater. Inter.*, 9 (2017) 16221-16227.
18. Kwon, H. T., Kim, J. H., Jeon, K. J., Park, C. M., "Co_xP compounds: electrochemical conversion/partial recombination reaction and partially disproportionated nanocomposite for Li-ion battery anodes", *RSC Adv.*, 4 (2014) 43227.
19. Khayyat, S. Z., Khayyat, S. V., "Removal of mercury (II) from wastewater by magnetic solid phase extraction with polyethylene glycol (PEG)-coated Fe_3O_4 nanoparticles", *J. Nanosci. Nanotechnol.*, 14 (2018) 65-70.
20. Lei, C. J., Wang, F. F., Yang, J., Gao, X. F., Yu, X. Y., Yang, B., Chen, G. H., Yuan, C., Lei, L. C., Hou, Y., "Embedding Co_2P nanoparticles in N-doped carbon nanotubes grown on porous carbon polyhedral for high-performance lithium-ion batteries", *Ind. Eng. Chem. Res.*, 57 (2018) 13019-13025.
21. Jin, R., Li, X. F., Sun, Y. X., Shan, H., Fan, L. L., Li, D. J., Sun, X. L., "Metal-organic frameworks-derived Co_2P@N-C@RGO with dual protection layers for improved sodium storage", *ACS Appl. Mater. Inter.*, 10 (2018) 14641-14648.
22. Sun, L., Xie, J., Zhang, L., Jiang, R. Y., Wu, J., Fan, L. L., Shao, R., Chen, Z. D., Jin, Z., "2D black TiO_{2-x} nanoplate-decorated Ti_3C_2 MXene hybrids for ultrafast and elevated stable lithium storage", *FlatChem*, 20 (2020) 100152.
23. Guo, Y. Y., Yuan, P. F., Zhang, J. N., Xia, H. C., Cheng, F. Y., Zhou, M. F., Li, J., Qiao, Y. Y., Mu, S. C., Xu, Q., "Co_2P-CoN double active centers confined in N-doped carbon nanotube: heterostructural engineering for trifunctional catalysis toward HER, ORR, OER, and Zn-air batteries driven water splitting", *Adv. Funct. Mater.*, (2018) 1805641.
24. Zhou, D., Fan, L. Z., "Co_2P nanoparticles encapsulated in 3D porous N-doped carbon nanosheet networks as an anode for high-performance sodium-ion batteries", *J. Mater. Chem. A*, 6 (2018) 2139-2147.
25. Zhu, G. Y., Ma, L. B., Lin, H. N., Zhao, P. Y., Wang, L., Hu, Y., Chen, R. P., Chen, T., Wang, Y. R., Tie, Z. X., Jin, Z., "High-performance Li-ion capacitor based on black-TiO_{2-x}/graphene aerogel anode and biomass-derived microporous carbon cathode", *Nano Research*, 12 (2019) 1713-1719.
26. Zhu, G. Y., Chen, T., Wang, L., Ma, L.B., Hu, Y., Chen, R. P., Wang, Y. R., Wang, C. X., Yan, W., Tie, Z. X., Liu, J., Jin, Z., "High energy density hybrid lithium-ion capacitor enabled by Co_3ZnC@N-doped carbon nanopolyhedra anode and microporous carbon cathode", *Energy Storage Materials*, 14 (2018) 246-252.
27. Zhu, G., Zhang, X. J., Li, Y. J., Zhao, G. Z., Xu, H. F., Jin, Z., "A carbon-coated shuttle-like $Fe_2O_3/Fe_{1-x}S$ heterostructure derived from metal-organic frameworks with high pseudocapacitance for ultrafast lithium storage", *Nanoscale Advances*, 2 (2020) 5201-5208.
28. Zheng, S. S., Guo, X. T., Xue, H. G., Pan, K. M., Liu, C. S., Pang, H., "Facile one-pot generation of metal oxide/hydroxide@metal–organic framework composites: highly efficient bifunctional electrocatalysts for overall water splitting", *Chemical Communications*, 55 (2019) 10904-10907.
29. Lv, T. T., Liu, Y. L., Wang, H., Yang, S. Y., Liu, C. S., Pang, H., "Crystal water enlarging the interlayer spacing of ultrathin $V_2O_5{\cdot}4VO_2{\cdot}2.72H_2O$ nanobelts for high-performance aqueous zinc-ion battery", *Chemical Engineering Journal*, 411 (2021) 128533.
30. Lv, T. T., Luo, X., Yuan, G. Q., Yang, S. Y., Pang, H., "Layered VO_2@N-doped carbon composites for high-performance rechargeable aqueous zinc-ion batteries", *Chemical Engineering Journal*, 428 (2022) 131211.
31. Das, D., Nanda, K. K., "One-step, integrated fabrication of Co_2P nanoparticles encapsulated N,P dual-doped CNTs for highly advanced total water splitting", *Nano Energy*, 30 (2016) 303-311.
32. Xu, K., Ding, H., Zhang, M. X., Chen, M., Hao, Z. K., Zhang, L. D., Wu, C. Z., Xie, Y., "Regulating water-reduction kinetics in cobalt phosphide for enhancing HER catalytic activity in alkaline solution", *Adv. Mater.*, (2017) 1606980.
33. Guo, H. P., Ruan, B. Y., Liu, L. L., Zhang, L., Tao, Z. L., Chou, S. L., Wang, J. Z., Liu, H. K., "Capillary-induced Ge uniformly distributed in N-doped carbon nanotubes with enhanced li-storage performance", *Small*, (2017) 1700920.
34. Shen, L. F., Lv, H. F., Chen, S. Q., Kopold, P., Aken, P. A., Wu, X. J., Maier, J., Yu, Y., "Peapod-like Li_3VO_4/N-doped carbon nanowires with pseudocapacitive properties as advanced materials for high-energy lithium-ion capacitors", *Adv. Mater.*, 29 (2017) 1700142.
35. Lim, E., Jo, C., Kim, H., Kim, M., Mun, Y., Chun, J., Ye, Y., Wang, J. H., Ha, K., Roh, K. C., Kang, K., Yoon, S., Lee, J., "Facile synthesis of Nb_2O_5@carbon core-shell nanocrystals with controlled crystalline structure for high-power anodes in hybrid supercapacitors", *ACS Nano*, 9 (2015) 7497-7505.

36. Chen, Z., Augustyn, V., Wen, J., Zhang, Y., Shen, M., Dunn, B., Lu, Y., "High-performance supercapacitors based on intertwined CNT/V_2O_5 nanowire nanocomposites", *Adv. Mater.,* 23 (2011) 791-795.
37. Banerjee, A., Upadhyay, K. K., Puthusseri, D., Aravindan, V., Madhavi, S., Ogale, S., "MOF-derived crumpled-sheet-assembled perforated carbon cuboids as highly effective cathode active materials for ultra-high energy density Li-ion hybrid electrochemical capacitors (Li-HECs)", *Nanoscale,* 6 (2014) 4387.
38. Que, L. F., Wang, Z. B., Yu, F. D., Gu, D. M., "3D ultralong nanowire arrays with a tailored hydrogen titanate phase as binder-free anodes for Li-ion capacitors", *J. Mater. Chem. A,* 4 (2016) 8716-8723.
39. Wang, Y. K., Liu, M. C., Cao, J. Y., Zhang, H. J., Kong, L. B., Trudgeon, D. P., Li, X. H., Walsh, F. C., "3D hierarchically structured CoS nanosheets: Li^+ storage mechanism and application of the high-performance lithium-ion capacitors", *ACS Appl. Mater. Interfaces,* 12 (2020) 3709-3718.